Editors' Suggestion

Edge-Induced Shear Banding in Entangled Polymeric Fluids

Ewan J. Hemingway and Suzanne M. Fielding
Department of Physics, Durham University, Science Laboratories, South Road, Durham DH1 3LE, United Kingdom

(Received 26 January 2018; published 30 March 2018)

Despite decades of research, the question of whether solutions and melts of highly entangled polymers exhibit shear banding as their steady state response to a steadily imposed shear flow remains controversial. From a theoretical viewpoint, an important unanswered question is whether the underlying constitutive curve of shear stress σ as a function of shear rate $\dot{\gamma}$ (for states of homogeneous shear) is monotonic, or has a region of negative slope, $d\sigma/d\dot{\gamma} < 0$, which would trigger banding. Attempts to settle the question experimentally via velocimetry of the flow field inside the fluid are often confounded by an instability of the free surface where the sample meets the outside air, known as "edge fracture." Here we show by numerical simulation that in fact even only very modest edge disturbances—which are the precursor of full edge fracture but might well, in themselves, go unnoticed experimentally—can cause strong secondary flows in the form of shear bands that invade deep into the fluid bulk. Crucially, this is true even when the underlying constitutive curve is monotonically increasing, precluding true bulk shear banding in the absence of edge effects.

DOI: 10.1103/PhysRevLett.120.138002

Polymeric fluids display exotic nonlinear rheological (deformation and flow) properties, stemming from the complicated underlying dynamics of their constituent entangled chainlike molecules. When subject to an imposed shear, for example, they commonly exhibit a heterogeneous flow response in which bands of differing shear rates form, with layer normals in the flow-gradient direction. This phenomenon of "shear banding" has been widely observed during the transient, time-dependent process, whereby a steady flowing state is established out of an initial rest state, following the switch on of a flow [1–3] or load [2–4], and in the perpetually time-dependent protocol of large amplitude oscillatory shear [5,6]. It has been successfully captured [7–12] in rheological constitutive models based on molecular theories [13,14] of polymer dynamics that posit the dominant mode of stress relaxation to be one of "reptation," in which any molecule snakes out of an effective tube formed from entanglements with its neighbors.

Perhaps surprisingly, the more basic question of whether shear bands form the ultimate steady flowing state in entangled polymers remains intensely controversial, despite decades of research. From a theoretical viewpoint, an important issue concerns whether the underlying constitutive curve of shear stress σ as a function of shear rate $\dot{\gamma}$ (for states of stationary homogeneous shear) is monotonically increasing, or instead has a region of negative slope, $d\sigma/d\dot{\gamma} < 0$. The latter would necessarily imply homogeneous shear to be unstable, leading to bulk banding in the steady flowing state. While the original reptation theory [14] predicted nonmonotonicity, more recent extensions to it incorporating the additional molecular processes of convective constraint release and chain stretch relaxation [15–17] can, at least in principle, restore monotonicity and (in melts) eliminate steady state banding. (In solutions with a strong enough coupling between flow and concentration fluctuations, steady state banding has been predicted to occur even if the constitutive curve is monotonic [18–21].) Whether they do so in practice, however, depends on the number of entanglements per molecule and on the level of convective constraint release, which is *a priori* unknown.

Just as this debate remains unsettled theoretically, studies aimed at resolving it experimentally have likewise proved controversial. The experimentally measured flow curve $\sigma(\bar{\dot{\gamma}})$ is always monotonically increasing but with a characteristically rather flat region spanning, typically, 1–4 decades in shear rate [4,22–25], depending on the fluid in question. Whether the underlying constitutive curve $\sigma(\dot{\gamma})$ is itself monotonic is not settled simply by measuring the flow curve, however, because a nonmonotonic constitutive curve would lead to shear banding, which restores a monotonic flow curve $\sigma(\bar{\dot{\gamma}})$ for the composite banded flow, with $\bar{\dot{\gamma}}$ the shear rate averaged across the bands. (For homogeneous flow, $\bar{\dot{\gamma}} = \dot{\gamma}$ everywhere, and the constitutive curve and flow curve coincide.)

The question of whether shear bands are present must therefore instead be investigated by explicit velocimetric studies of the flow field inside the sample. Tapadia and Wang [26] gave evidence for steady state shear banding in entangled polymer solutions, suggesting a nonmonotonic underlying constitutive curve. In contrast, Hu *et al.* [23] observed shear banding only transiently during shear startup, giving way at longer times to homogeneous shear,

suggesting a monotonic constitutive curve. Later work on more highly entangled samples did however report long-lived shear bands in some experimental runs, but not in others [4], even (in some cases) when repeated for the same imposed loads or flow rates.

While the aim in these velocimetry experiments is to measure the fluid's true bulk flow behavior, in practice all rotational shear rheometers have a free surface where the fluid sample meets the outside air. Care is obviously then needed to measure the flow field as far into the sample as possible, at a depth from the surface that is many multiples of the gap width between the shearing plates. Even then, however, polymeric fluids are known to be highly susceptible to "edge fracture" [27–30], in which this free surface between the fluid sample and air destabilizes when the fluid is sheared. This can lead to secondary flows penetrating some depth into the bulk. Indeed, edge fracture was discussed as a possible source of the variability between runs mentioned above [4]. Significant possible edge fracture in experiments concerning the presence or absence of shear banding in entangled polymers has likewise been discussed extensively in Refs. [22,24,31–36].

In this Letter, we report, for the first time, simulations exploring the complicated dynamical interplay between these surface and bulk instabilities in sheared polymeric fluids. Our principal contributions are threefold. First, we show that only modest deformations of the sample edge—which are the precursors of true edge fracture but may (in themselves) go unnoticed—can indeed lead to secondary flows that penetrate some distance into the fluid bulk. Second, for a material with a bulk constitutive curve that is rather flat (but still monotonically increasing, e.g., comparable to that measured experimentally in Ref. [23]), these secondary flows can be very strong, and they can furthermore invade the bulk to up to depths of 10–20 gap widths in from the sample edge, which is the maximum depth typically attained experimentally due to the finite aspect ratio of any sample. Third, these secondary flows take the form of shear bands. Importantly, this is true despite the constitutive curve being monotonic in our simulations, precluding true bulk shear banding in the absence of any surface disturbance. This Letter therefore shows that only modest precursors of the surface transition of edge fracture can precipitate a strong quasibulk shear banding effect far into the sample.

As shown in Fig. 1, we consider a planar slab of fluid sheared at rate $\bar{\dot{\gamma}}$ between hard walls at $y = 0, L_y$. The flow direction is denoted $\hat{\mathbf{x}}$ and the flow-gradient direction $\hat{\mathbf{y}}$. The surfaces of the fluid sample in the vorticity direction $\hat{\mathbf{z}}$ are in contact with the air. The sample length in that direction (in the initial unsheared state) is Λ. Our simulation box has length L_z, with periodic boundary conditions in z. (Only its left half is shown in Fig. 1.) At the plates we impose boundary conditions of no slip and no permeation. Translational invariance is assumed in x.

The total stress $\mathbf{T}$ in any fluid element is taken to comprise an isotropic contribution with pressure p, a Newtonian contribution characterized by a viscosity η, and a slow viscoelastic contribution $\mathbf{\Sigma}$ from the polymer chains. The Newtonian part models contributions from both the background solvent, and also from fast intrachain polymeric relaxation modes. We assume conditions of creeping flow, with the force balance condition $\boldsymbol{\nabla}\cdot\mathbf{T} = 0$. This gives $\eta\boldsymbol{\nabla}^2\mathbf{v} + \boldsymbol{\nabla}.\mathbf{\Sigma} - \boldsymbol{\nabla}p = 0$ inside the fluid and $\eta_a\boldsymbol{\nabla}^2\mathbf{v} - \boldsymbol{\nabla}p = 0$ in the outside air, with η_a the air viscosity. The pressure field $p(\mathbf{r}, t)$ is determined by enforcing incompressible flow, such that the velocity field $\mathbf{v}(\mathbf{r}, t)$ obeys $\boldsymbol{\nabla}\cdot\mathbf{v} = 0$. The dynamics of the viscoelastic stress $\mathbf{\Sigma}$ is taken to obey the diffusive Giesekus model [37]:

$$D_t\mathbf{\Sigma} = 2G\mathbf{D} + \mathbf{\Sigma}\cdot\boldsymbol{\nabla}\mathbf{v} + \boldsymbol{\nabla}\mathbf{v}^{\mathrm{T}}\cdot\mathbf{\Sigma} - \frac{1}{\tau}(\mathbf{\Sigma} + \alpha\mathbf{\Sigma}^2) + D\boldsymbol{\nabla}^2\mathbf{\Sigma}, \tag{1}$$

in which $D_t\mathbf{\Sigma} \equiv \partial_t\mathbf{\Sigma} + \mathbf{v}.\boldsymbol{\nabla}\mathbf{\Sigma}$ captures Galilean invariance; $\boldsymbol{\nabla}\mathbf{v}_{\alpha\beta} = \partial_\alpha v_\beta$ and $\mathbf{D} = \frac{1}{2}(\boldsymbol{\nabla}\mathbf{v} + \boldsymbol{\nabla}\mathbf{v}^T)$. The first three terms on the rhs of Eq. (1) capture the loading of viscoelastic stress in an imposed flow. The next capture relaxation on a time scale τ, back towards an unstressed state, with α characterizing the apparent change in relaxation rate as the chains become anisotropically aligned in flow. The final diffusive term ensures that the structure of the interface between any shear bands that form is properly accounted for [38]. To test that our results are robust to choice of constitutive model, we have verified that the physical picture reported below also holds in the diffusive Johnson-Segalman model [39] (results not shown).

The air-fluid coexistence is captured via a phase field (Cahn-Hilliard) approach [40,41], with a mobility M for air-fluid intermolecular diffusion, a scale G_μ for the free energy density of demixing, and a slightly diffuse air-fluid interface of thickness l. This gives an interfacial tension $\Gamma = 2\sqrt{2}G_\mu l/3$. In having a diffuse interface, our simulations are capable of capturing any motion of the contact line along the wall that arises in flow [41]. Our numerical scheme is described in Ref. [30].

We choose units of length in which the gap width $L_y = 1$, of time, in which the viscoelastic relaxation time $\tau = 1$, and of stress, in which the viscoelastic modulus $G = 1$. We set the equilibrium contact angle of the fluid-air interface at the plates $\theta = 90°$, and we have checked that our findings are robust to variations in this quantity. We set the inverse air gap size $L_y/(L_z - \Lambda) = 0.25$, the air-fluid interface width $l/L_y = 0.01$, the inverse mobility for intermolecular diffusion, $l^2/MG_\mu\tau = 0.01$–0.1, the stress diffusivity $D = 10^{-4}$, and the air viscosity $\eta_a/G\tau = 0.006$–0.02; all converged to their appropriate small limit, along with the numerical grid and time steps.

Important physical quantities to be explored are the dimensionless surface tension $\Gamma/GL_y = \Gamma$, the sample

aspect ratio $\Lambda/L_y = \Lambda$, Newtonian viscosity $\eta/G\tau = \eta$, and imposed shear rate $\bar{\dot{\gamma}}\tau = \bar{\dot{\gamma}}$. Among these, we vary the viscosity η in order to vary the shape of the underlying constitutive curve $\sigma(\dot{\gamma})$, for a fixed value of the anisotropy parameter $\alpha = 0.8$. (We could instead have fixed η and varied α, and we have checked that this gives the same physical picture as that reported below.) In particular, the width of the plateau region of the constitutive curve will prove an important quantity in what follows. Accordingly, we define the extrema of the plateau region as the shear rates $\dot{\gamma}_h$, $\dot{\gamma}_l$ that correspond to $\pm 5\%$ of the stress at the flattest point, then quantify the plateau width via their logarithmic difference $n = \log(\dot{\gamma}_h/\dot{\gamma}_l)$. We shall report our phase diagrams below both in terms of the viscosity $\eta - \eta_c$ (where $\eta_c = 0.005918$ is the value below which the constitutive curve is nonmonotonic) and n; the latter is directly set by the former (for our fixed α), and is the more directly accessible quantity experimentally.

The surface tension Γ and the second normal stress $T_{yy} - T_{zz} = N_2(\bar{\dot{\gamma}})$, which depends on the imposed shear rate $\bar{\dot{\gamma}}$, together control the tendency or otherwise of the fluid-air interface to show edge fracture, as explored in Refs. [27,30]. For a fixed shear rate, the interface is stable at high surface tension Γ. At intermediate Γ, the interface bows modestly but remains otherwise intact. We define the degree of bowing d as the difference between the rightmost and leftmost z positions of the interface, as shown in Fig. 1. At low Γ, full edge fracture occurs, with a catastrophic interfacial breakup that would signal the end of any reliable experimental run. Here we focus on the intermediate regime, with modest edge bowing that is a precursor to full edge fracture, but might well (in itself) go unnoticed experimentally. Typical orders of magnitude of $\Gamma = \Gamma/GL_y$ are 0.001–0.1 for synthetic polymers and 0.1–10.0 for DNA solutions [2,4,23,42–44].

We now present our results. The basic phenomenon that we report is exemplified by the snapshots of Fig. 1. Only modest bowing of the fluid-air interface is apparent in each case, consistent with the preceding remark. However, radically different bulk behavior is seen between the two snapshots. This can be explained by the differing shape of their underlying constitutive curves. The upper snapshot pertains to the moderately sloping constitutive curve (a) of Fig. 2 (left). In this case, the disturbance at the sample edge has virtually no effect on the bulk. In contrast, the lower snapshot pertains to the flatter constitutive curve (b) in Fig. 2. Here, any perturbations caused by the modest disturbance at the sample edge are strongly amplified by the flatness of the constitutive curve to cause a strong shear banding effect in the shear rate $\tilde{\dot{\gamma}} = \sqrt{2\mathbf{D}:\mathbf{D}}$, which invades far into the bulk, many gap widths in from the sample edge. Crucially, this is true despite the constitutive curve being monotonically increasing, precluding true bulk shear banding in the absence of edge effects.

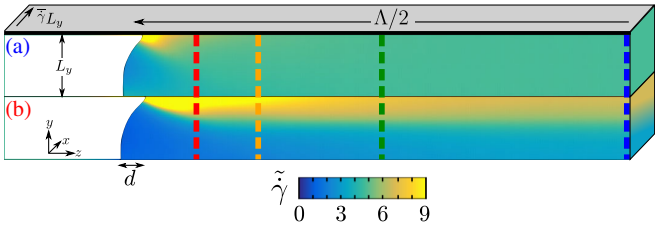

FIG. 1. Shear-rate colormaps in the steady flowing state. Top: A fluid with the moderately sloping constitutive curve shown as (a) in Fig. 2 (left) exhibits homogeneous bulk flow. Bottom: A fluid with the flatter constitutive curve (b) in Fig. 2 (left) shows strong apparent quasibulk shear banding. Dashed colored lines show positions at which the velocity profiles of Fig. 2 (right) are taken. Parameters: $\Lambda = 16.0$, $\bar{\dot{\gamma}} = 4.7$, $\Gamma = 0.16$ with $\eta = 0.02$, 0.006 giving $n = 0.45$, 1.06 (top, bottom).

To further exemplify this behavior, we show in Fig. 2 (right) the velocity profiles $v_x(y)$ measured at depths $z = 1, 2, 4, 8L_y$ into the sample from the fluid-air interface. For the snapshot of Fig. 1 (top), these all show near homogeneous shear, with the local shear rate $\dot{\gamma} = \partial v_x/\partial y$ independent of y, apart from some weak heterogeneity in the profile very close to the sample edge, $z = L_y$. In contrast, for the lower snapshot of Fig. 1, the velocity profiles show noticeable shear banding that persists many gap widths in from the sample edge. For use below, we note that the "degree of banding" can be quantified for any such profile as $\Delta_{\dot{\gamma}} = (\dot{\gamma}_{\max} - \dot{\gamma}_{\min})/\bar{\dot{\gamma}}$, with $\dot{\gamma}_{\max}$ the maximum shear rate at any point across y (which occurs at $y = 0$ in Fig. 2, right), and $\dot{\gamma}_{\min}$ the minimum (which occurs at $y = 1.0$). $\bar{\dot{\gamma}}$ is the gap-averaged value. By inspecting many profiles, we conservatively adopt $\Delta^c_{\dot{\gamma}} = 0.15$ as the minimum threshold for visually obvious banding.

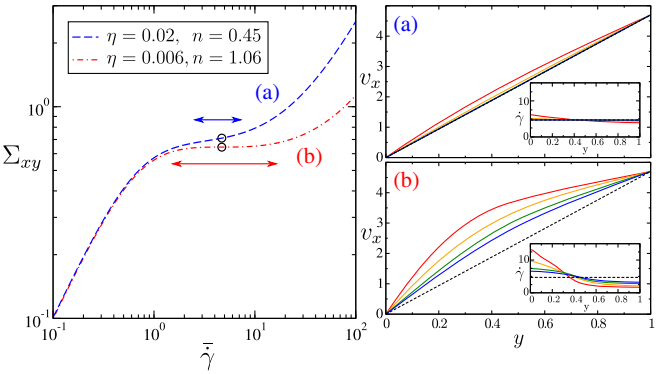

FIG. 2. Left: Constitutive curves for (a) moderately and (b) strongly shear thinning fluids, with Newtonian viscosities $\eta = 0.02$ and 0.006 giving plateau widths $n = 0.45$ (blue arrow) and 1.06 (red arrow), respectively. The shear rate to which the snapshots in Fig. 1 correspond is shown by the circles. Right: Plots of the velocity profiles (and, inset, shear rate profiles) pertaining to the snapshots of Fig. 1 at the depths $z = 1, 2, 4, 8L_y$ into the sample from the free surface, for $\eta = 0.02$ ($n = 0.45$) (top) and $\eta = 0.006$ ($n = 1.06$) (bottom).

So far, we have presented results for a single value of the surface tension Γ, separately for a moderately sloping constitutive curve (larger η) and a flatter curve (smaller η), with an imposed shear rate $\bar{\dot{\gamma}}$ near the flattest part of the constitutive curve in each case. We now explore more fully the behavior as a function of $\Gamma, \bar{\dot{\gamma}}$ and η. To do so, we present in Fig. 3 (bottom) colorscales of the degree of banding $\Delta_{\dot{\gamma}}$ at the cell midpoint $z = 8.0$ for a sample of length $\Lambda = 16.0$. The right panel shows results for $\eta = 0.006$ [which we recall gives the flatter constitutive curve (b) with plateau width $n = 1.06$ in Fig. 2, (left)] in the plane $\Gamma, \bar{\dot{\gamma}}$ of surface tension, and imposed shear rate. (So this panel explores a range of shear rates across one particular constitutive curve.) The left panel shows results in the plane Γ, n of surface tension, and the parameter $n(\eta)$ that characterizes the shape of the constitutive curve, for a fixed imposed shear $\bar{\dot{\gamma}} = 4.7$, near the flattest part of the constitutive curve in each case. (So, this panel explores a collection of constitutive curves with increasingly broad plateau regions for increasing n leftwards along the horizontal axis.) The corresponding panels in Fig. 3 (top) show the degree of bowing d of the fluid-air interface, each directly counterpart to the degree of banding in the panel underneath.

The top panels confirm the scenario discussed above from Ref. [30]. For any given imposed shear rate $\bar{\dot{\gamma}}$, the fluid-air interface is undisturbed for high surface tension Γ, with zero interfacial bowing, $d = 0$. For lower values of the surface tension, below the red thick line, the interface bows modestly when the sample is sheared, giving $d = O(L_y)$. (For lower surface tensions still, not shown in Fig. 3, full fracture occurs, giving a catastrophic breakup of the interface.) It is important to note, however, that the degree of interfacial bowing d does not appear to vary significantly with the overall shape of the constitutive curve as prescribed by η in the top left panel, once comfortably inside the unstable region.

The degree of shear banding in the plane of surface tension and strain rate in the bottom right panel of Fig. 3 pertains to the flatter constitutive curve (b) of Fig. 2 (left). As can be seen, the region of visually apparent banding (as enclosed by the thick black line) arises for shear rates $\bar{\dot{\gamma}} = 2.0$–9.0, in the flattest region of the constitutive curve. For the fixed strain rate $\bar{\dot{\gamma}} = 4.7$ in the flattest part, the degree of banding as a function of surface tension, and the overall shape of constitutive curve is shown in the bottom left panel of Fig. 3. A clear relation is seen here between the increasing breadth n of the plateau region in the constitutive curve (leftwards along the horizontal axis), and the increasing degree of shear banding many gap-widths into the sample. This is true even though the degree of fluid-air interfacial bowing (top left panel) does not vary much with increasing n, as emphasized above. This is important, because it shows that strong quasibulk shear banding can arise for highly shear thinning fluids, even with a monotonically increasing constitutive curve, even given only modest bowing of the fluid-air interface.

So far, we have presented results for one particular sample length $\Lambda = 16.0$, for the degree of banding at its cell midpoint $z = 8.0$. In Fig. 4, we explore the degree of banding as a function of the position z in from the sample edge, for a range of different cell sizes. The left panel shows

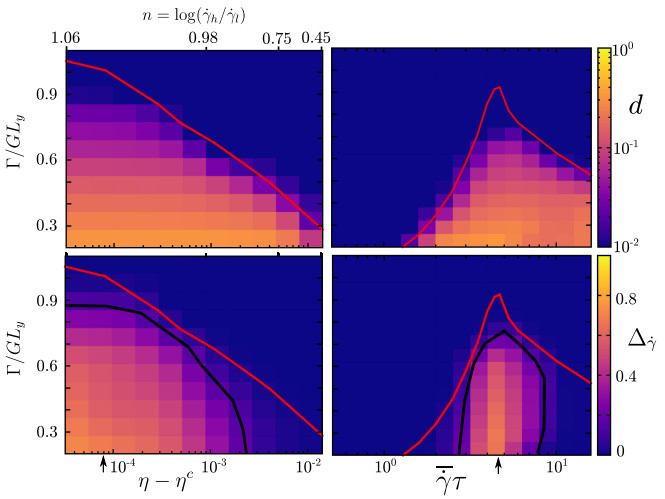

FIG. 3. Colormaps of (top) the degree of bowing d of the air-fluid interface and (bottom) the degree of shear banding $\Delta_{\dot{\gamma}}$ at the cell midpoint $z = 8.0$ for a sample of length $\Lambda = 16.0$. These are shown (left) in the plane of surface tension and $\eta - \eta_c$ (bottom x-axis label) or equivalently $n(\eta)$ (top x-axis label, characterizing the width of the flattest part of the constitutive curve), for a shear rate $\bar{\dot{\gamma}} = 4.7$ near its flattest part; and (right) in the plane of surface tension and imposed shear rate $(\Gamma, \bar{\dot{\gamma}})$ for a fixed $\eta = 0.006$ ($n = 1.06$), which gives a rather flat constitutive curve. The red lines show the onset of the edge fracture instability, and black lines show the contour $\Delta_{\dot{\gamma}}^c = 0.15$.

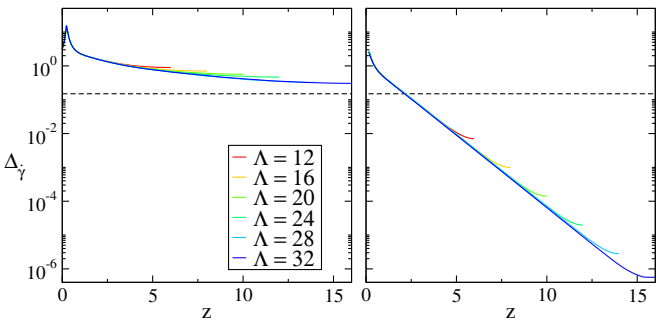

FIG. 4. Normalized degree of banding $\Delta_{\dot{\gamma}}$ as a function of distance z in from the sample edge, from $z = 0$ up to the cell midpoint, for several different sample lengths Λ. (Left) For a fluid with a relatively flat constitutive curve, $\eta = 0.006$ ($n = 1.06$), and (right) for a fluid with a moderately sloping constitutive curve, $\eta = 0.02$ ($n = 0.45$). In each case, $\bar{\dot{\gamma}} = 4.7$ and $\Gamma = 0.2$. The horizontal dashed line shows the threshold $\Delta_{\dot{\gamma}}^c = 0.15$ for visually apparent shear banding.

results for the case of the relatively flat constitutive curve (b) in Fig. 2 (left), and the right panel shows results for the moderately sloping constitutive curve (a) in Fig. 2. (In each case, the imposed shear rate is near the flattest part of the constitutive curve.) As can be seen, for the moderately sloping constitutive curve (Fig. 4, right), the degree of banding falls below the threshold for being visually apparent by a distance of about 2–3 gap widths in from the sample edge. In contrast, for the flatter constitutive curve (Fig. 4, left), the degree of banding stays above the threshold for being visually apparent even at the cell centerpoint $z = 16.0L_y$ for the longest sample length $\Lambda = 32.0L_y$. This is towards the limit of experimental sample aspect ratios, and indeed, it is larger than the depth from the fluid-air surface at which the velocimetry is usually performed experimentally.

To summarize, in shear thinning polymeric fluids, we have shown that only modest disturbances of the sample edge (which are the precursors of true edge fracture but might well in themselves go unnoticed experimentally) can lead to strong shear banding that invades far into the fluid bulk, even for the largest sample sizes that are typically studied experimentally. Importantly, this is true even for an underlying constitutive curve that is monotonically increasing, precluding true bulk banding in the absence of edge effects. This work therefore shows that strong quasibulk shear banding can be precipitated by even only modest precursors of the surface transition of edge fracture.

The research leading to these results has received funding from the European Research Council under the EU's 7th Framework Programme (FP7/2007-2013)/ERC Grant No. 279365. The authors thank Mike Cates for a critical reading of the manuscript.

[1] S. Ravindranath, S.-Q. Wang, M. Olechnowicz, and R. P. Quirk, Macromolecules **41**, 2663 (2008).
[2] P. E. Boukany and S.-Q. Wang, Soft Matter **5**, 780 (2009).
[3] P. E. Boukany and S.-Q. Wang, J. Rheol. **53**, 73 (2009).
[4] Y. T. Hu, J. Rheol. **54**, 1307 (2010).
[5] P. Tapadia, S. Ravindranath, and S.-Q. Wang, Phys. Rev. Lett. **96**, 196001 (2006).
[6] S. Shin, K. D. Dorfman, and X. Cheng, Phys. Rev. E **96**, 062503 (2017).
[7] J. M. Adams and P. D. Olmsted, Phys. Rev. Lett. **102**, 067801 (2009).
[8] J. M. Adams, S. M. Fielding, and P. D. Olmsted, J. Rheol. **55**, 1007 (2011).
[9] R. L. Moorcroft and S. M. Fielding, Phys. Rev. Lett. **110**, 086001 (2013).
[10] K. A. Carter, J. M. Girkin, and S. M. Fielding, J. Rheol. **60**, 883 (2016).
[11] R. L. Moorcroft and S. M. Fielding, J. Rheol. **58**, 103 (2014).
[12] G. Ianniruberto and G. Marrucci, J. Rheol. **61**, 93 (2017).
[13] A. E. Likhtman and R. S. Graham, J. Non-Newtonian Fluid Mech. **114**, 1 (2003).
[14] M. Doi and S. F. Edwards, *The Theory of Polymer Dynamics*, International Series of Monographs on Physics (Clarendon Press, Oxford, 1988).
[15] G. Ianniruberto and G. Marrucci, J. Non-Newtonian Fluid Mech. **65**, 241 (1996).
[16] G. Ianniruberto and G. Marrucci, J. Rheol. **45**, 1305 (2001).
[17] R. S. Graham, A. E. Likhtman, T. C. B. McLeish, and S. T. Milner, J. Rheol. **47**, 1171 (2003).
[18] S. M. Fielding and P. D. Olmsted, Phys. Rev. Lett. **90**, 224501 (2003).
[19] S. M. Fielding and P. D. Olmsted, Eur. Phys. J. E **11**, 65 (2003).
[20] M. Cromer, M. C. Villet, G. H. Fredrickson, and L. G. Leal, Phys. Fluids **25**, 051703 (2013).
[21] S. Hooshyar and N. Germann, Phys. Fluids **28**, 063104 (2016).
[22] C. Sui and G. B. McKenna, Rheol. Acta **46**, 877 (2007).
[23] Y. T. Hu, L. Wilen, A. Philips, and A. Lips, J. Rheol. **51**, 275 (2007).
[24] Y. Li and G. B. McKenna, Rheol. Acta **54**, 771 (2015).
[25] P. Tapadia and S.-Q. Wang, Macromolecules **37**, 9083 (2004).
[26] P. Tapadia and S.-Q. Wang, Phys. Rev. Lett. **96**, 016001 (2006).
[27] R. I. Tanner and M. Keentok, J. Rheol. **27**, 47 (1983).
[28] C. S. Lee, B. C. Tripp, and J. J. Magda, Rheol. Acta **31**, 306 (1992).
[29] M. Keentok and S.-C. Xue, Rheol. Acta **38**, 321 (1999).
[30] E. J. Hemingway, H. Kusumaatmaja, and S. M. Fielding, Phys. Rev. Lett. **119**, 028006 (2017).
[31] T. Schweizer and M. Stockli, J. Rheol. **52**, 713 (2008).
[32] Y. Li, M. Hu, G. B. McKenna, C. J. Dimitriou, G. H. McKinley, R. M. Mick, D. C. Venerus, and L. A. Archer, J. Rheol. **57**, 1411 (2013).
[33] S.-Q. Wang, G. Liu, S. Cheng, P. E. Boukany, Y. Wang, and X. Li, J. Rheol. **58**, 1059 (2014).
[34] Y. Li, M. Hu, G. B. McKenna, C. J. Dimitriou, G. H. McKinley, R. M. Mick, D. C. Venerus, and L. A. Archer, J. Rheol. **58**, 1071 (2014).
[35] P. E. Boukany, S.-Q. Wang, S. Ravindranath, and L. J. Lee, Soft Matter **11**, 8058 (2015).
[36] S.-Q. Wang, Rheol: Open Access **1**, 104 (2017).
[37] H. Giesekus, J. Nonnewton. Fluid Mech. **11**, 69 (1982).
[38] C.-Y. David Lu, P. D. Olmsted, and R. C. Ball, Phys. Rev. Lett. **84**, 642 (2000).
[39] M. W. Johnson Jr. and D. Segalman, J. Nonnewton. Fluid Mech. **2**, 255 (1977).
[40] D. M. Anderson, G. B. McFadden, and A. A. Wheeler, Annu. Rev. Fluid Mech. **30**, 139 (1998).
[41] H. Kusumaatmaja, E. J. Hemingway, and S. M. Fielding, J. Fluid Mech. **788**, 209 (2016).
[42] T. Schweizer, Rheol. Acta **46**, 629 (2007).
[43] E. Ricci, R. Sangiorgi, and A. Passerone, J. Colloid Interface Sci. **102**, 295 (1984).
[44] S. Skorski and P. D. Olmsted, J. Rheol. **55**, 1219 (2011).